Visualizing an convergence of three mitochondrial molecule mRNAs for DRP1/MFN2/UCP4 on soma of cerebellar Purkinje cells by RNAscope

Hui Liu
Air Force Medical University
Tingting Luo
Air Force Medical University
Feifei Wu
Air Force Medical University
Baolin Guo
Air Force Medical University
Kunlong Zhang
Air Force Medical University Xijing Hospital: Xijing Hospital
Shujiao Li
Air Force Medical University
Xiaodong Li
Air Force Medical University Xijing Hospital: Xijing Hospital
Ruiqing Wang
Air Force Medical University
Jinghao Chen
Air Force Medical University Xijing Hospital: Xijing Hospital
Lu Wang
Yan'an University
Yanling Yang
Air Force Medical University Xijing Hospital: Xijing Hospital
Ya-Yun Wang (wangyy@fmmu.edu.cn)
Air Force Medical University https://orcid.org/0000-0003-3578-467X

Research Article

Keywords: Mitochondrial dynamic proteins, RNAscope, Purkinje cell, Cerebellum, Cre-LoxP mice

Posted Date: August 19th, 2021

DOI: https://doi.org/10.21203/rs.3.rs-818426/v1

Abstract

We know little about how mitochondrial dynamic are regulated in the Purkinje cells. To explore it, we first set up a transgenic mice in which Purkinje cells expressed tdTomato in the cerebellum of Gad2-cre;ZsGreen-tdTomatofl/fl mice. Secondly Double stainings verified tdTomato cells were Calbinin (CB)-positive Purkinje cells, but not colocalized either with astrocyte marker GFAP or with microglia marker Iba1. Thirdly, application of RNAscope in situ hybridization with the identification of mRNAs of mitochondrial fusion (Mfn2), calcium transporter (Mcu and Nclx) and uncoupling proteins (Ucp2 and Ucp4) were used onto Purkinje cells for specific spatial analysis. The RNAscope assay used a semi-quantitative H scoring guideline to evaluate the staining results. The number of bins ranges from 0–4 according to the ACD scoring system. Moreover, ACD scoring system was used to calculate the overall H scores of Dendritic Weighted Formula (DWF) and Soma Weighted Formula (SWF). Our data for the first time demonstrated that Mfn2 mRNAs expression was evident in Prukinje cells with the H scores of DWF and SWF as 60 and 139, respectively. And few Ucp4 mRNAs expression was present in dendritic shafts of Prukinje cells with the H scores of DWF and SWF as 14 and 103, respectively. It should be noted that Mcu mRNAs, Nclx mRNAs, as well as Ucp2 mRNAs expression were only scattered on both soma and dendrites in Prukinje cells with the low H scores of DWF and SWF. Double RNAscope profiling of mitochondrial molecules showed The data showed Mfn1 mRNAs are present only in the soma of the Purkinje cells, instead of processes. Double RNAscope showed almost none of dots of Drp1 mRNAs was co-localized with dots of Mcu mRNAs, as well as almost none of dots of Ucp2 mRNAs was co-localized with dots of Mfn2 mRNAs. All of these results show the mitochondrial Drp1/Mfn2/UCP4 convergence on the Purkinje cells. Finally, a major focus of present research will be to develop new and more specific molecules that tune the activity of the Purkinje cells activate or inactivate and to address diseases for which such druglike molecules may open therapeutic windows for Purkinje cells-related manipulation in the clinic. The molecular identification of drug targets, mechanism of action, and structural basis of their activity will crucially enable preclinical development.

1 Introduction

Purkinje cells are the sole output of the computational circuitry of the cerebellar cortex and provide the signals required for motor planning, execution and coordination in their rate of firing and pattern of activity (Louis ED and Faust PL, 2020). Malfunction of these neurons often results in cerebellar ataxia: a disorder characterized by poor balance, loss of posture and difficulties in performing rapid coordinated movements (Pan MK et al., 2020; Kostadinov D et al., 2019). Purkinje cells fire spontaneously with highly regular pacemaking and their relayed neurotransmission depend on more than 150,000 excitatory and inhibitory synapses (Kostadinov D et al., 2019). So Purkinje cells have a particular dependence on precise control of mitochondrial dynamics.

Mitochondria are dynamic double-membrane-bound organelles that are associated with ATP generation, calcium regulation, and the biosynthesis of aminoacids, lipids, and nucleotides (Patron M et al., 2018). Progress in the field of mitochondrial biology in the past few years has shown that mitochondrial

activities have important implications for the cerebellum (Fecher C et al., 2019). Mitochondrial fusion and fission, calcium buffering handling, and uncoupling process are crucial for functional maintain of Purkinje cells (Cunnane SC et al., 2020). Understanding these mechanisms will enable discovery and development of new strategies for Purkinje cell related treatment.

Although there is clearly an emerging link between mitochondrial defects and Purkinje cells, its molecular basis is poorly understood. Which mitochondrial fusion and fission proteins affect the mitochondria of Purkinje cells, and how about mitochondrial calcium buffering proteins and uncoupling proteins? To examine the distribution pattern of mitochondrial moleculars in purkinje cells, we used cre-loxP system to generate a conditional knock-in mice with specific fluorescence in GABAergic purkinje cell. In the Gad2-ires-Cre mice, all of GABAergic neurons contained Cre recombinase. In ZsGreen-tdTomatofl/f mice, the green fluorescent protein ZsGreen and the red fluorescent protein tdTomato were knocked into the mice and the loxP sites were buried on both sides of ZsGreen. After crossing of these two mice, the Purkinje cells could be easily identified as red fluorescent protein under confocal microscopy. These mice were then used for the following immunofluorescence and hybridization.

By using RNAscope in situ hybridization, we found an convergence of mRNAs for three mitochondrial molecules, Drp1/Mfn2/UCP4, on the Purkinje cells. Surprisingly, two mitochondrial calcium buffering proteins of MCU and NCLX, another fusion protein Mfn1, as well as another mitochondrial uncoupling protein UCP2 could not be found abundantly in the Purkinje cells. Our results indicate that the DRP1/MFN2-dependent fission and fusion on mitochondrial outer membrane, as well as UCP4-dependent ROS regulation on mitochondrial inner membrane are a fundamental, targetable determinant of Purkinje cell. Our work provides a framework for understanding mitochondrial plasticity at Purkinje cell level, and could suggest ways of modulating mitochondrial activity to treat cerebellum-related diseases. In addition, we think that visualization of gene expression with Purkinje cells-specific spatial context can be achieved by combining the highly sensitive and specific RNAscope in situ hybridization with Gad2-cre;ZsGreen-tdTomato$^{fl/fl}$ mice.

2 Materials And Methods

2.1 Animals and mouse breeding

To examine the distribution pattern of mitochondrial moleculars in purkinje cells, we used cre-*loxP* system to generate a conditional knock-in mice with specific fluorescence in GABAergic purkinje cell.

The C57BL/6-Gad2$^{EM1(IRES-ICRE-PA)SMOC}$ (named as Gad2-ires-Cre) mice were purchased from Institute of Model Zoology, Nanjing University with the Product Number of D000668, previously reported (Taniguchi H et al., 2011). It is well-known that GABA (g-aminobutyric acid) in mammals was synthesized by two glutamic acid decarboxylase (GAD) GAD67 and GAD65 (Fish KN et al., 2021). These two proteins were encoded by Gad1 and Gad2 genes. The Gad2-ires-Cre mice inserted an internal ribosome entry site (ires)

and a Cre recombinase sequence at the 3' end of the Gad2 allele, so that all of GABAergic neurons contained Cre recombinase.

The *loxP*-flanked (floxed) ZsGreen-tdTomato mice used here are *B6/JGpt-H11*$^{em1Cin(CAG\text{-}LoxP\text{-}ZsGreen\text{-}Stop\text{-}LoxP\text{-}tdTomato)/Gpt}$ mice (ZsGreen-tdTomato$^{fl/fl}$), which were purchased from Jiangsu Jicui Yaokang Biological Technology Co. Ltd with the Product Number of E2101190037, reported previously (Muzumdar MD et al., 2007). In ZsGreen-tdTomato$^{fl/f}$ mice, the green fluorescent protein ZsGreen and the red fluorescent protein tdTomato were knocked into the mice H11 gene site and the *loxP* sites were buried on both sides of ZsGreen.

After crossing of these two mice, all GABAergic neurons in the newly generated transgenic Gad2-cre; ZsGreen-tdTomato$^{fl/fl}$ mice would transfer from expressing green fluorescence to expressing red fluorescence protein due to Cre recombinase cutting loxP sites. Therefore, Purkinje cells, a typical GABAergic subneurons in the brain of Gad2-cre; ZsGreen-tdTomato$^{fl/fl}$ mice, could be easily identified under confocal microscopy. These mice were then used for the following immunofluorescence labeling and single RNAscope in situ hybridization.

It should be indicated that the normal adult C57BL/6 mice were used for double RNAscope in situ hybridizations.

All of the mice are kept in a barrier facility, and all animal experiments were conducted in accordance with the procedures approved by the Ethical Committee of the Air Force Medical University and followed the institutional guidelines for the use of laboratory animals..

Animals were housed at a constant 23 °C in a 12 h light/dark cycle (lights off at 20:00), with food and water available ad libitum. nts. The day of birth was considered as postnatal day 0 (P0).

2.2 Genotyping

Genotype was identified by PCR with genomic DNA obtained from the tails. The primers sequences and PCR programs were listed in **Table 1.**

2.3 Immunofluorescence labeling

To verify the reliability of red tdTomato fluorescence within Purkinje cell in the generated Gad2-cre;ZsGreen-tdTomato$^{fl/fl}$ mice, immunofluorescence labeling was conducted according to the methods described previously (Huang J et al., 2008) with minor modifications.

Six eight-week male Gad2-cre;ZsGreen-tdTomato$^{fl/fl}$ mice were perfused transcardially with 0.1 M phosphate buffer (PB; pH 7.4) containing 4% paraformaldehyde. The whole cerebellum were obtained and postfixed with the same fixative for 4 h, placed in 30% (w/v) sucrose reliability solution in 0.05 M PB solution (PBS; pH 7.4) overnight at 4 °C, and cut into sagittally 30 mm thick sections on a freezing microtome. Then the cerebellum sections were mounted onto the slides and incubated in 0.01 M PBS

supplemented with 3% hydrogen peroxide for 10 min to block endogenous peroxidase and then in a blocking buffer containing 5% BSA/10% normal goat serum/0.25% Triton X-100 for 60 min at room temperature to prevent nonspecific staining. Following this, the sections were incubated in the blocking buffer for 60 min at room temperature and then in a solution containing primary antibodies of the marker of Purkinje cells (Calbindin, CB), the marker of granular cells (NeuN), the marker of astrocytes (GFAP), the marker of microglia (Iba1) **(Table 2)** from different species simultaneously for 18 h at 4 °C. After washing, sections were incubated with appropriate secondary antibodies **(Table 2)** for 2 h at room temperature.

It should be indicated that in the cerebellum of Gad2-cre;ZsGreen-tdTomato$^{fl/fl}$ mice, Purkinje cells expressed bright tdTomato fluorescence, while non-GABAergic expressed bright ZsGreen fluorescence. So we observed the sections under a confocal laser scanning microscope (FV-1000, Olympus, Tokyo, Japan) with a confocal depth of 1.0 mm. The mode of triple immunofluorescence labelings was used. The laser beams and filters for ZsGreen were the 488 nm of excitation and 525 nm of emision, the parameters for tdTomato were 550 nm of excitation and 570 nm of emision, and for the antibody stained were 649 nm of excitation and 670 nm of emision. Around 30 slices obtained from 6 mice (5 slices per mouse) were randomly chosen. Images were carried out by individuals blinded towards the experimental groups.

2.4 Imaris file format description of immunofluorescence labeling

In order to more accurately imaging three-dimensional (3D) structure of GABAergic Purkinje cells expressing red fluorescence in the cerebellum of Gad2-cre;ZsGreen-tdTomato$^{fl/fl}$ mice, Imaris × 64 image analysis software (version 9.6.0, Oxford Instruments, England) was used. The Imaris file had high performance rendering and processing of laser confocal images. The Path Attribute Description was /DataSet/ResolutionLevel 0/TimePoint 0/Channel 0 with informations concerning resolution 0, time point 0 and channel 0. ImageSizeX = 285, indicating the size in X in pixel for Resolution Level 0; ImageSizeY = 218, indicating the size in Y in pixel; ImageSizeZ = 64, indicating the size in Z in pixe.

2.5 Single and double RNAscope in situ hybridization

To provide Purkinje cells-specific spatial analysis about the RNAs profiling of important mitochondrial moleculars, the single RNAscope technology (Wang F et al., 2012) was conducted on the cerebellum sections from the Gad2-cre;ZsGreen-tdTomato$^{fl/fl}$ mice. Moreover, in order to verify the characterization of the molecules, we conducted double RNAscope assays to simultaneously detect two targets on the normal mice section.

2.5.1 Probes

The probes used in RNAscope were divided into two types: first for molecules on outer mitochondrial membrane (OMM) including DRP1 (mitochondrial fission protein), MFN1 and MFN2 (mitochondrial fusion protein); second for molecules on the inner mitochondrial membrane (IMM) including MCU (mitochondrial calcium intruder), NCLX (mitochondrial calcium intruder), UCP2 and UCP4 (mitochondrial

uncoupling protein); the negative (dapB) and positive (Polr2a/PPIB/UBC) controls; whose information were provided in **Table 3**.

2.5.2 Tissue preparation

RNAscope® Multiplex Fluorescent Reagent Kit manual was performed as instructed by Advanced Cell Diagnostics (ACD). Newly prepared 1× phosphate buffered saline (PBS, pH 7.4) and 4% paraformaldehyde (PFA, pH 7.4) were used to perfuse the heart of mice. Tissues of interest were then removed in 4% PFA at 4˚C for 24 hours, and then treated with sucrose solutions for dehydration. The tissues were cryostat-sectioned at 15μm onto SuperFrost Plus charged slides. Sections were only briefly thawed to adhere to the slide but were immediately returned to the -20˚C cryostat chamber until completion of sectioning. Before used for following histology, The slides were baked in chamber at 37˚C for 3 hours. Slides were removed from baking chamber and immediately transferred to 1× PBS at room temperature for 5 minutes. Each slide was incubated with Hydrogen peroxide at room temperature for 10 minutes. After washed by distilled water, the slides were treated by the boiled target retrieval solutions at 96˚C for 10 minutes. The tissues were placed in distilled water immediately at room temperature, and then dehydrated in 100% ethanol for 3 minutes. The slides were air-dried briefly and then boundaries were drawn around each section using a hydrophobic pen (CIRISC PAP pen, I.S. CIRCLE WRITER, Japan). When hydrophobic boundaries had dried, protease III reagent was added to each section until fully covered, incubation at 40˚C for 30 minutes. During this period, slides were placed in a prewarmed humidity control tray containing dampened filter paper in the HybEZ oven (ACD).

2.5.3 Hybridization

Each slide was then added only one probe or a mixture of two probes. Channel 1, Channel 2, and Channel 3 probes (50: 1: 1 dilution, as directed by ACD due to stock concentrations), which were pipetted onto each section until fully submerged. This was performed one slide at a time to avoid liquid evaporation and section drying. The humidity control tray was placed in a HybEZ oven (ACD) for 2 hours at 40˚C. A table of all the probes used is shown in **Table 3**. After probe incubation, the slides were washed twice in 1× RNAscope® wash buffer and returned to the oven for 30 minutes after submersion in AMP-1 reagent. Washes and amplification were repeated using AMP-2, and AMP-3 reagents with a 30-, and 15-minute incubation period, respectively. HRP-C1 signal, HRP-C2 signal, and HRP-C3 signal were developed respectively. Different dyes were needed to differentiate probes deriving from three kinds of channels. We employed Opal 520 (FP1487001KT, PerkinElmer) to mark channel 1 probes, Opal 570 (FP1488001KT, PerkinElmer) to mark channel 2 probes, and Opal 690 (FP1497001KT, PerkinElmer) to mark channel 3 probes. Slides were incubated with DAPI for 5 minutes before being washed, air-dried, and coverslipped with Prolong Gold Antifade mounting medium.

2.6 RNAscope images acquisition and semi-quantitative analysis

Anatomical structures were analyzed in sagittal sections and mapped according to Paxinos and Franklin atlas (Paxinos G and Franklin KBJ., 2001) and Allen map (http://mouse.brain-

map.org/static/atlas)**.** Fluorescent signals of mRNA hybridization for mitochondrial molecules were imaged with a 10×, 20×, 40× and 60× objective lens on a a confocal laser scanning microscope (FV-1000, Olympus, Tokyo, Japan). All microscope and camera settings were identical for all images. We used the ImageJ64 software (National Institute of Health. Bethesda, MD, USA), as previously described (Fe Lanfranco M et al., 2017).

The RNAscope assay used a semi-quantitative H scoring guideline to evaluate the staining results. We scored the number of dots per Purkinje cell rather than the signal intensity to interpret RNAscope staining, because the number of dots correlates to the number of RNA copy numbers, whereas dot intensity reflects the number of probe pairs bound to each molecule (Gebara E et al., 2021). In the present study, H score was to visualize the dynamic expression level by binning the percentage of cells with a certain expression level or number of dots in one bin. The number of bins ranges from 0 - 4 according to the ACD scoring system. The overall H score can range from 0 - 400 and is calculated as shown:

$$\text{H-score} = \sum_{\substack{Bin \\ 0->4}} (\text{ACD score or bin number x percentage of cells per bin})$$

Negative control (dapB) stained slides were always imaged at the settings used for target probe imaging and did not result in appreciable signal. Positive control (Polr2a/PPIB/UBC) should be indicated as successful staining which have a score ≥2.

2.7 Statistical analysis

Figures for RNAscope and Immunofluorescence labeling are representative of sections obtained from three animals. Data for Figure 4, expressed as the mean ± SEM (sections obtained from five animals), were analyzed using one-way analysis of variance (ANOVA) with Bonferroni's multiple comparison post hoc test using GraphPad Prism software v.5.0 (Graphpad). A *p*-value < 0.05 was considered statistically significant.

3 Results

3.1 Characteristic of tdTomato cells in GAD2-cre;ZsGreen-tdTomatofl/fl mice

Firstly, we used a Cre-*loxP* strategy to generate a conditional knock-in mice with specific fluorescence in GABAergic Purkinje cell **(Fig. 1A)**. The Gad2-ires-Cre mice inserted a Cre recombinase sequence at Gad2 allele to make all GABAergic neurons containing Cre recombinase.

So in the ZsGreen-tdTomato$^{fl/f}$ mice, ZsGreen and tdTomato were knocked in and the *loxP* sites were buried on both sides of ZsGreen. After crossing of these two mice, all GABAergic neurons would transfer from expressing ZsGreen to expressing tdTomato due to Cre recombinase cutting loxP sites. The genotyping strategy used four sets of primers to produce four bands of 1465 bp (for ZsGreen-tdTomato

with loxP site), 285 bp (for wild type site), 352 bp (for Cre recombinase), and 250 bp (for wild type site) **(Fig. 1B)**.

Secondly, average body appearances were compared between control Gad2-cre mice and the Gad2-cre;ZsGreen-tdTomato$^{fl/fl}$ mice **(Fig. 1C)**. Interestingly and apparently, Gad2-cre;ZsGreen-tdTomato$^{fl/fl}$ mice showed dazzling green light visible to the naked eye in external auricle skin (arrow), plantar skin (arrow), as well as perianal skin (arrow), although the body weights of both types of mice had no significant difference. Moreover, the brains of Gad2-cre;ZsGreen-tdTomato$^{fl/fl}$ mice showed green fluorescence, while the brains of control Gad2-cre mice showed normal pink, which made it very easy to distinguish the GABAergic knock-in mice.

Thirdly, the confocal microscope images were taken to show that Purkinje cells expressed tdTomato in the cerebellum of Gad2-cre;ZsGreen-tdTomato$^{fl/fl}$ mice, while non-GABAergic cells expressed ZsGreen **(Figs. 1D and 1E)**. We could find that the neuronal bodies of Prukinje cells with red fluorescence (asterisk marked in **Fig. 1E**) were aligned like dominos stacked throughout the PCL (purkinje cell layer), also they had large dendritic arbors (**Fig. 1E**) like within the molecular layer (ML) and sent axons like bright flame out off cerebellar cortex (**Fig. 1E**), therefore they left the dark area of granular layer (GCL) which were occupied by green non-GABAergic cells (**Fig. 1E**).

Fourthly, the Imaris file was designed to allow better visualization of Purkinje cells specifically expressed tdTomato fluorescence in GAD2-cre;ZsGreen-tdTomato$^{fl/fl}$ mice **(shown in Videos. 1-3)**. We could see that the neuronal bodies of Prukinje cells with red fluorescence were aligned like dominos stacked throughout the PCL, while the dark area of granular layer (GCL) were occupied by green non-GABAergic cells.

3.2 Double stainings verified tdTomato cells were Purkinje cells

Previous studies have shown that Cerebellar Purkinje cells could be marked by Calbinin (CB) (Singh-Bains MK et al., 2019), while the granular cells be marked by NeuN (Yawno T et al., 2019). In addition, the astrocytes (as GFAP as marker) (Levite M et al., 2020) and microglia (as Iba1 as marker) (Janakiraman U et al., 2020) were believed to be scattered throughout the cerebellar cortex. So, in order to verify the cells expressing tdTomato fluorescence in cerebellum of Gad2-cre;ZsGreen-tdTomato$^{fl/fl}$ mice were exclusively Purkinje cells, the present immunostainings with the four antibodies mentioned above were observed under the psudo blue color. The percentage of blue cells in the distinct cell subgroups was determined.

It could be indicated that dominos stacked - like tdTomato-positive cells (red) were 95.0% colocalized with CB (green) **(Fig. 2A)**, so that they appeared the color of purple. On the contrary, immunostaing data showed few of tdTomato-positive cells were colocalized with NeuN, the marker of granular cells **(Fig. 2B)**. Moreover, almost none of tdTomato-positive cells were colocalized either with astrocyte marker GFAP **(Fig. 2C)** or with microglia marker Iba1 **(Fig. 2D)**.

At the same time, ZsGreen-positive cells were densely distributed cross GCL, scattered though PCL, and few in ML **(Fig. 2)**. Double stainings showed almost none of these green cells were colocalized with

Purkinje cell marker CB **(Fig. 2A).** On the contrary, these green cells were mainly consist of NeuN-positive granular cells **(Fig. 2B)**. Our results also confirmed that ZsGreen-positive cells were not astrocyte **(Fig. 2C)** or microglia **(Fig. 2D)**.

These data suggested that tdTomato-positive cells were primarily expressed in GABAergic Purkinje cells within cerebellar cortex. Then, RNAscope in situ hybridization was performed to examine the presences of seven mitochondrial proteins within the Purkinje cells of Gad2-cre;ZsGreen-tdTomato$^{fl/fl}$ mice.

3.3 Application of RNAscope in situ hybridization onto GAD2-cre;ZsGreen-tdTomatofl/fl mice for Purkinje cell - specific spatial analysis

Identification of mRNAs of mitochondrial fusion (Mfn2), calcium transporter (Mcu and Nclx) and uncoupling proteins (Ucp2 and Ucp4) in Purkinje cells in the cerebellar cortex of GAD2-cre;ZsGreen-tdTomato$^{fl/fl}$ mice with RNAscope probes. Red cells were Purkinje cells; green cells were non-GABAergic cells; blue dots were RNA fluorescence. Moreover, ACD scoring system was used to calculate the overall H scores of Dendritic Weighted Formula (DWF) and Soma Weighted Formula (SWF).

3.3.1 Mfn2 mRNA

Mitofusin 2 (Mfn2) control the fusion of the outer mitochondrial membrane (OMM), but the physiological function of Mfn2 in Purkinje cells remains unclear. Our data firstly demonstrated that *Mfn2* mRNAs expression was evident in Prukinje cells in cerebellum of Gad2-cre;ZsGreen-tdTomato$^{fl/fl}$ mice **(Fig. 3A)**. Moreover, 76.5% dendrite shafts were ranked as Bin 1 because they only had 1-3 dots per shaft **(Fig. 3B)**; On the contrary, 71.8% soma were ranked as Bin 4 because they had more than 15 dots per cell body **(Fig. 3C)**. The overall H scores of DWF and SWF were calculated as 60 and 139, respectively **(Table 4)**.

3.3.2 *Mcu* mRNA

Mitochondrial Ca^{2+} uptake is mediated by the Mitochondrial Calcium Uniporter (MCU) complex, located on the inner mitochondrial membrane (IMM). Our data confirmed the previous report (Fecher C et al., 2019) that few *Mcu* mRNAs expressions were present on Prukinje cells in cerebellum of Gad2-cre;ZsGreen-tdTomato$^{fl/fl}$ mice **(Fig. 3D)**. About Moreover, 57.1% dendrite shafts were ranked as Bin 0 because they had no dot per shaft **(Fig. 3E)**; Similarly, 58.1% soma were also ranked as Bin 1 **(Fig. 3F)**. The overall H scores of DWF and SWF were high as 70 and 22, respectively **(Table 4)**.

3.3.3 *Nclx* mRNA

Conversely to MCU, Ca^{2+} release is under the control of the Na^{+}/Ca^{2+} exchanger, encoded by the NCLX gene, located on IMM. Our data firstly demonstrated that *Nclx* mRNAs expression were only scattered on both soma and dendrites in Prukinje cells in cerebellum of Gad2-cre;ZsGreen-tdTomato$^{fl/fl}$ mice **(Fig. 3G)**. About 91.7% dendrite shafts were ranked as Bin 0 because they had no dot per shaft **(Fig. 3H)**; Similarly,

58.3% soma were ranked as Bin 1 because they had only no more than 3 dots per cell body **(Fig. 3I)**. The overall H scores of DWF and SWF were 4 and 31, respectively **(Table 4)**.

3.3.4 *Ucp2* mRNA

UCP2 are IMM proteins that may regulate mitochondrial energy metabolism and ROS generation. Our data firstly demonstrated that unexpectedly, few *Ucp2* mRNAs expression was present in Prukinje cells in cerebellum of Gad2-cre;ZsGreen-tdTomato$^{fl/fl}$ mice **(Fig. 3J)**. Moreover, 75.0% dendrite shafts and 41.2% soma were ranked as Bin 0 because they had no dot **(Figs. 3K and 3L)**. The overall H scores of DWF and SWF were only 15 and 27, respectively **(Table 4)**.

3.3.5 *Ucp4* mRNA

UCP4, another IMM protein for regulating mitochondrial energy metabolism and ROS generation, has been looked like a twin of UCP2. Our data confirmed that few *Ucp4* mRNAs expression was present in dendritic shafts of Prukinje cells in cerebellum of Gad2-cre;ZsGreen-tdTomato$^{fl/fl}$ mice **(Fig. 3M)**. However, 67.6% soma were ranked as Bin 3 because they had 10-15 dots per cell body **(Figs. 3N and 3O)**. The overall H scores of DWF and SWF were only 14 and 103, respectively **(Table 4)**.

3.4 Double RNAscope profiling of mitochondrial molecules in cerebellar cortex of normal mice

In order to verify the characterization of the molecules, we conducted double RNAscope assays to simultaneously detect two targets on the normal mice section.

3.4.1 *Mfn1* (green) and *Pcp2* (red)

Because our present *Mfn1* probe was not suitable for the detection in the samples from GAD2-cre;ZsGreen-tdTomato$^{fl/fl}$ mice, we did double RNAscope profiling of *Mfn1* mRNA (green) in Purkinje cells (red) which were distinguished by the red fluorescence with the mRNA probe of Purkinje cell protein-2 (pcp2) gene **(Fig. 4A)**. Higher magnification images showed that within the PCL, some dots could be found in the soma of Purkinje cells (red) **(Fig. 4B)**. However, within both the ML and the GCL, few green dots could be found in the dendrites or axons of Purkinje cells, respectively **(Fig. 4B)**. ACD quantification confirmed the middle-level expression level of *Mfn1* mRNAS in soma **(Fig. 4C)**. The calculation of the percent of double *Pcp2-Mfn1* stainings on single *Pcp2*-positive expressions confirmed the very low colocalization both in the ML and in the GCL **(Fig. 4D)**. The data suggested Mfn1 mRNAs are present only in the soma of the Purkinje cells, instead of processes.

3.4.2 *Drp1* (green) and *Mcu* (red)

Because our previous report had presented the detailed distribution of Drp1 mRNA in the cerebellar cortex of normal mice by in situ hybridization method, the present double RNAscope profiling was to verify the distribution of *Mcu* in Purkinje cells because these cells could be distinguished by Drp1 fluorescence **(Fig. 5A)**. Higher magnification images confirmed that green *Drp1*-positive dots could outline the soma of

Purkinje cells **(Fig. 5B)**. Our results of Gad2-cre;ZsGreen-tdTomato$^{fl/fl}$ mice by in situ hybridization had showed that a number of dots of *Mcu* mRNAs were present in processes and soma of Prukinje cells **(Fig. 3D)**. Here, the double RNAscope profiling was consistent with the previous distribution pattern. Unexpectedly and interestingly, almost none of dots of *Drp1* mRNAs was co-localized with dots of *Mcu* mRNAs, wherever at ML, PCL or GCL **(Fig. 5C).** The data suggested the separation of Drp1 on OMM and Mcu on IMM even they were all abundant in the Purkinje cells.

3.4.3 *Ucp2* (green) and *Mfn2* (red)

Our results of Gad2-cre;ZsGreen-tdTomato$^{fl/fl}$ mice by RNAscope in situ hybridization had showed that a number of dots of *Mfn2* mRNAs were present in soma of Prukinje cells, although this kind of high level did not happen in dendrites of Purkinje cells **(Figs. 3A-3C)**. On the contrary, the dots of *Ucp2* mRNAs were only scattered not only on the soma but also on the dendrites of Prukinje cells **(Figs. 3J-3L)**. The present double RNAscope profiling confirmed the dense expressions of *Mfn2* in soma of the Purkinje cells **(Fig. 6A),** so that in the higher magnification images these cells could be distinguished by *Mfn2* red fluorescence **(Fig. 6B)**. Moreover, unsurprisingly, almost none of dots of *Ucp2* mRNAs was co-localized with dots of *Mfn2* mRNAs **(Fig. 6C)**. The data verified the presence of *Mfn2* but the nonexistence of *Ucp2* on the Purkinje cells.

4 Discussion

To explore the mitochondrial mechanisms of Purkinje cells, we first set up a transgenic mice in which Purkinje cells could be distinguished easily by expressing red fluorescence. We then detected spatial RNA profiling of seven mitochondrial molecules, including dynamin-related protein-1 (Drp1), mitochondrial calcium uniporter (MCU); mitofusion 1 and 2 (Mfn1/2), sodium/lithium/calcium exchanger (NCLX), and uncoupling protein 2 and 4 (UCP2/4), by RNAscope combined with ACD quantification. We finally proposed a mitochondrial Drp1/Mfn2/UCP4 convergence on the Purkinje cells, which would make up a mitochondrial quality control system. Our results establish a framework for understanding the pathogenic mechanism underlying cerebellum-related neurological diseases.

4.1 Drp1/Mfn1/Mfn2

Mitochondrial fission and fusion play critical roles in creating new mitochondria and removing damaged mitochondria. In mammalian cells, fission/fusion events are mainly mediated by several large dynamin-related GTPase proteins, including conserved dynamin-related GTPase (Drp1), conserved dynamin-related GTPase mitofusion 1 and 2 (Mfn1 and 2), and optic dominant atrophy 1 (Opa1). Our lab have published the data previously about the expression of Drp1 at high level on the soma of cerebellum Purkinje cells by the combination of immunohistochemistry and in situ hybridization on GAD67 (glutamic acid decarboxylase 67) - GFP (green fluorescent protein) transgenic mice (Luo TT et al., 2020). The present findings have confirmed the distribution pattern of Drp1 on Purkinje cells. These data suggest that the mitochondrial fission in Purkinje cells may be dependent on the mitochondrial fission mediator, Drp1. In

fact, mitochondrial fission mediated by the GTPase Drp1 is an attractive drug target in neurodegenerative disorders (Chandra R et al., 20107; Bordt EA et al., 2017). Basal Drp1-dependent mitochondrial fission is required for mitochondrial trafficking to synapses, mitochondrial quality control, and brain development (Ishihara N et al., 2009; Wakabayashi J et al., 2009; Kageyama Y et al., 2014). Drp1 is highly conserved and contains many critical functional features that correspond to specific target structures within the enzyme, such as GTP binding, GTP hydrolysis, self-assembly and protein interactions with key functions in mitochondrial division (Frank S, et al., 2001; Lackner LL and Nunnari J, 2010). While the fission defects may limit mitochondrial motility, decrease energy production, promote oxidative stress and lead to accumulating of mtDNA defects, thereby promoting neuronal dysfunction and cell death (Grohm J et al., 2012; Oettinghaus B, et al., 2012). Thus, regardless of the different upstream stress stimulus, Drp1-mediated mitochondrial fragmentation and downstream mitochondrial pathways play a major role for the fate of Purkinje cells. Significantly, Drp1 must be an efficient strategy for the neuroprotection against multiple cerebellar damage.

The finding of dense distribution of Mfn2 on Purkinje cells deserves high attention for four reasons. First, the mutations in Mfn2 have been found to cause a human neurodegeneration disease, Charcot-Marie-Tooth neuropathy type 2A (Chen H et al., 2007; Züchner S et al., 2004; Chung KW et al., 2006; Ishikawa K et al., 2019). Second, our data have supported previous paradigm that Mfn2 is expressed at significantly greater levels in Purkinje cells than is Mfn1 (Chen H et al., 2007). Third, it has been reported that Purkinje cells require Mfn2 but not Mfn1 for cell survival and dendritic outgrowth (Chen H et al., 2007; Züchner S et al., 2004; Chung KW et al., 2006). Fourth, Mfn2-deficient Purkinje cells have shown impaired respiratory complex activity and defects in inner membrane structure characteristic of respiratory dysfunction (Chen H et al., 2007). Our RNAscope studies provide insight into the dependence of the fusion of outer mitochondrial membrane (OMM) of soma of Purkinje cells on the molecular Mfn2.

In fact, neurodegeneration in neurodegenerative diseases has been related to several mitochondrial dynamics imbalances such as excessive fragmentation of mitochondria, impaired mitophagy, and blocked mitochondrial transport in axons. Our findings raise the intriguing possibility that a convergent pathway underlies the pathogenesis of neurodegenerative disorders. Nonetheless, the exact role of Drp1/Mfn2-dependent mitochondrial dynamics in Purkinje cells requires further investigation.

4.2 MCU and NCLX

Mitochondrial Ca^{2+} homeostasis plays a central role in nervous system. Previous studies have suggested that dysfunction of Ca homeostasis is associated with oxidative stress and many neurological diseases (Rizzuto R et al., 2012; Giorgi C et al., 2018; Fan M et al., 2020; Baughman JM et al., 2011; De Stefani D et al., 2015; Peng TI and Jou MJ, 2015; Owens K et al., 2013; Di Lisa F and Bernardi P, 2009; Zhang L et al., 2019). In the last 5 years, most of the molecules that control mitochondrial Ca^{2+} homeostasis have been finally identified. Mitochondrial Ca^{2+} uptake is mediated by the Mitochondrial Calcium Uniporter (MCU) complex, a macromolecular structure that guarantees Ca^{2+} accumulation inside

mitochondrial matrix upon increases in cytosolic Ca^{2+}. Conversely, Ca^{2+} release is under the control of the Na^{+}/Ca^{2+} exchanger, encoded by the NCLX gene, and of a H^{+}/Ca^{2+} antiporter, whose identity is still debated (De Stefani D et al., 2016). Audrey Bonnan et al. have found that in Purkinje cells the dendritic Ca^{2+} transients are sufficient, potent triggers of plasticity induction that instruct the acquisition of cerebellar learning, by using optogenetics and animal behavioral tests (Bonnan A et al., 2021). In the present study, as expected, our results have confirmed the previous important conclusion (Fecher C et al., 2019) that very low level of MCU expressions were on Prukinje cells. At the same time, we have at the first time reported that the numbers of Dendritic Weighted Formula (DWF) and Soma Weighted Formula (SWF) were even lower as 4 and 31, respectively. If it were true, it would be reasonable to speculate that there is other mitochondrial calcium regulators, such as of a H^{+}/Ca^{2+}, antiporter which provides flexibility to the cerebellum. Our data pave a way to appreciate mitochondria in Purkinje cells as a highly cell-type-specific biology.

4.3 UCP2 and UCP4

Mitochondria take up Ca^{2+} through the mitochondrial calcium uniporter complex to regulate energy production, cytosolic Ca^{2+} signaling, and cell death (Rizzuto R et al., 2012; Giorgi C et al., 2018; Fan M et al., 2020). In mammals, the uniporter complex (uniplex) contains four core components: the pore-forming MCU, gatekeeper MICU1 and MICU2, and an auxiliary EMRE subunit essential for Ca^{2+} transport. Previous studies have suggested that MCU-regulated Ca homeostasis is associated with oxidative stress and many neurological diseases (Baughman JM et al., 2011; De Stefani D et al., 2015; Peng TI and Jou MJ, 2015; Owens K et al., 2013; Di Lisa F and Bernardi P, 2009; Zhang L et al., 2019). It has been found that in Purkinje cells the dendritic Ca^{2+} transients are sufficient, potent triggers of plasticity induction that instruct the acquisition of cerebellar learning, by using optogenetics and animal behavioral tests (Bonnan A et al., 2021). In the present study, we have found the high level of Mcu expression dots on dendrites (Fig. 4D), soma (Fig. 4D), even axons (Fig. 5) of Prukinje cells. In view of this, it is reasonable to speculate it is due to Mcu which provides flexibility to the cerebellum in its role in producing appropriate behavioral responses to different adaptive stimuli. Thus MCU has been confirmed to be a potential therapeutic target in neurological diseases in the future.

5 Conclusion

When applied to the purkinye cells of the cerebellum, our approach yielded a number of insights. First, our verified the convergence of mitochondrial proteins Drp1/Mfn2/MCU/UCP4 on the purkinje cells in situ. Second, we generated GAD2-cre;ZsGreen-tdTomatofl/fl mice to allow resolving of purkinje cell-specific mitochondrial changes under multiple pathological conditions because of their high-resolution imaging for purkinje cells, both by light microscopy and electron microscopy. Third, mitochondrial proteins topographical analysis of our cerebellar RNAscope resulted in clear predictions for differentially regulated mitochondrial dynamic mechanisms, which could be studied in the further research. Fourth, the lack of

Mfn1/Nclx/Ucp2 indicated the unique intracellular mitochondrial mechanisms in Purkinje cells related to the cell distinct morphology, firing pattern and synaptic plasticity.

Abbreviations

A: Axons; ACD, Advanced Cell Diagnostics; ANOVA, Analysis of variance; ATP, Adenosine-triphosphate; CB, Calbindin; D, Dendritic arbors; dapB, 4-hydroxy-tetrahydrodipicolinate reductase; DAPI, 2-(4-Amidinophenyl)-6-indolecarbamidine dihydrochloride; Drp1, Dynamin-related protein 1; DWF, Dendritic Weighted Formula; GABA, γ-aminobutyric acid; GAD, Glutamic acid decarboxylase; GCL, Granular layer; GFAP, Glial fibrillary acidic protein; IMM, Inner mitochondrial membrane; Mcu, Mitochondrial calcium uniporter; Mfn1, Mitofusion 1; Mfn2, Mitofusion 1; ML, Molecular layer; Nclx, Sodium/lithium/calcium exchanger; NeuN, Neuron specific nuclear protein; OMM, Outer mitochondrial membrane; PB, Phosphate buffer; PBS, Phosphate buffered saline; PCL, Purkinje cell layer; Pcp2, Purkinje cell protein 2; PCR, Polymerase chain reaction; PFA, Paraformaldehyde; Polr2a, RNA polymerase II subunit A; PPIB, Peptidylprolyl isomerase B; ROS, Reactive oxygen species; SWF, Soma Weighted Formula; UBC, Ubiquitin C; Ucp2, Uncoupling protein 2; Ucp4, Uncoupling protein 4.

Declarations

Competing interests

The authors declare no competing interests.

Authors' contributions

YY.W., YL.Y. and L.W designed the experiments. H.L. and TT.L.conducted the experiments. BL.G., KL.Z., SJ.L., XD.L. RQ.W. and JH.C. analyzed the data and participated in figures drawing. YY.W. and FF.W. wrote the manuscript. The authors read and approved the final manuscript.

Funding

This work was supported by the National Natural Science Foundation of China (81870415), Xijing Hospital Boosting Plan (XJZT19Z29), Military Medicine Upgrade Program of Air Force Military Medical University (2020SWAQ04), Health Services Project of Air Force Military Medical University (21WQ023), The project of science and technology to improve the combat effectiveness of school flight personnel (2019ZTC03) and Open Project of State Key Laboratory of Military Stomatology (2018KA01).

Acknowledgments

We thank all members of our lab for their helpful discussions and comments during the completion of this project.

Availability of data and materials

The datasets used and analyzed during the current study are available from YY.W. on reasonable request.

References

Baughman JM, Perocchi F, Girgis HS, Plovanich M, Belcher-Timme CA, Sancak Y, et al. (2011). Integrative genomics identifies MCU as an essential component of the mitochondrial calcium uniporter. *Nature* 476, 341-345. doi: 10.1038/nature10234.

Bonnan A, Rowan MMJ, Baker CA, Bolton MM, Christie JM. (2021). Autonomous Purkinje cell activation instructs bidirectional motor learning through evoked dendritic calcium signaling. *Nat Commun.* 12, 2153. doi: 10.1038/s41467-021-22405-8.

Bordt EA, Clerc P, Roelofs BA, Saladino AJ, Tretter L, Adam-Vizi V, et al.(2017). The Putative Drp1 Inhibitor mdivi-1 Is a Reversible Mitochondrial Complex I Inhibitor that Modulates Reactive Oxygen Species. *Dev Cell* 40, 583-594. doi: 10.1016/j.devcel.2017.02.020.

Chandra R, Engeln M, Schiefer C, Patton MH, Martin JA, Werner CT, et al. (2017). Drp1 Mitochondrial Fission in D1 Neurons Mediates Behavioral and Cellular Plasticity during Early Cocaine Abstinence. *Neuron* 96, 1327-1341. doi: 10.1016/j.neuron.2017.11.037.

Chen H, McCaffery JM, Chan DC. (2007). Mitochondrial fusion protects against neurodegeneration in the cerebellum. *Cell* 130, 548-562. doi: 10.1016/j.cell.2007.06.026.

Chung KW, Kim SB, Park KD, Choi KG, Lee JH, Eun HW, et al. (2006). Early onset severe and late-onset mild Charcot-Marie-Tooth disease with mitofusin 2 (MFN2) mutations. *Brain* 129, 2103-2118. doi: 10.1093/brain/awl174.

Cunnane SC, Trushina E, Morland C, Prigione A, Casadesus G, Andrews ZB, et al. (2020). Brain energy rescue: an emerging therapeutic concept for neurodegenerative disorders of ageing. *Nat Rev Drug Discov*. 19, 609-633. doi: 10.1038/s41573-020-0072-x.

De Stefani D, Patron M, Rizzuto R. et al. (2015). Structure and function of the mitochondrial calcium uniporter complex. *Biochim Biophys Acta*. 1853, 2006-2011. doi: 10.1016/j.bbamcr.2015.04.008.

De Stefani D, Rizzuto R and Pozzan T. (2016). Enjoy the Trip: Calcium in Mitochondria Back and Forth. *Annu Rev Biochem.* 85, 161-192. doi: 10.1146/annurev-biochem-060614-034216.

Di Lisa F and Bernardi P. (2009). A CaPful of mechanisms regulating the mitochondrial permeability transition. *J Mol Cell Cardiol*. 46, 775-780. doi: 10.1016/j.yjmcc.2009.03.006.

Fan M, Zhang J, Tsai CW, Orlando BJ, Rodriguez M, Xu Y, et al. (2020). Structure and mechanism of the mitochondrial Ca^{2+} uniporter holocomplex. *Nature* 582, 129-133. doi: 10.1038/s41586-020-2309-6.

Fecher C, Trovò L, Müller SA, Snaidero N, Wettmarshausen J, Heink S, et al. (2019). Cell-type-specific profiling of brain mitochondria reveals functional and molecular diversity. *Nat Neurosci.* 22, 1731-1742. doi: 10.1038/s41593-019-0479-z.

Fe Lanfranco M, Loane DJ, Mocchetti I, Burns MP, Villapol S. (2017). Combination of Fluorescent in situ Hybridization (FISH) and Immunofluorescence Imaging for Detection of Cytokine Expression in Microglia/Macrophage Cells. *Bio Protoc*. 7, e2608. doi: 10.21769/BioProtoc.2608.

Fish KN, Rocco BR, DeDionisio AM, Dienel SJ, Sweet RA, Lewis DA. (2021). Altered Parvalbumin Basket Cell Terminals in the Cortical Visuospatial Working Memory Network in Schizophrenia. *Biol Psychiatry.* 90, 47-57. doi: 10.1016/j.biopsych.2021.02.009.

Frank S, Gaume B, Bergmann-Leitner ES, Leitner WW, Robert EG, Catez F, et al. (2001). The role of dynamin-related protein 1, a mediator of mitochondrial fission, in apoptosis. *Dev Cell*. 1, 515-525. doi: 10.1016/s1534-5807(01)00055-7.

Gebara E, Zanoletti O, Ghosal S, Grosse J, Schneider BL, Knott G, et al. (2021). Mitofusin-2 in the Nucleus Accumbens Regulates Anxiety and Depression-like Behaviors Through Mitochondrial and Neuronal Actions. *Biol Psychiatry*. 89, 1033-1044. doi: 10.1016/j.biopsych.2020.12.003.

Giorgi C, Marchi S, Pinton P. (2018). The machineries, regulation and cellular functions of mitochondrial calcium. *Nat Rev Mol Cell Biol*. 19, 713-730. doi: 10.1038/s41580-018-0052-8.

Grohm J, Kim SW, Mamrak U, Tobaben S, Cassidy-Stone A, Nunnari J, et al. (2012). Inhibition of Drp1 provides neuroprotection in vitro and in vivo. *Cell Death Differ*. 19, 1446-1458. doi: 10.1038/cdd.2012.18.

Huang J, Wang Y, Wang W, Wei Y, Li Y, Wu S. (2008). Preproenkephalin mRNA is expressed in a subpopulation of GABAergic neurons in the spinal dorsal horn of the GAD67-GFP knock-in mouse. Anat Rec (Hoboken). 291, 1334-1341. doi: 10.1002/ar.20755.

Ishihara N, et al. (2009). Mitochondrial fission factor Drp1 is essential for embryonic development and synapse formation in mice. *Nat Cell Biol*. 11, 958-966. doi: 10.1038/ncb1907.

Ishikawa K, Yamamoto S, Hattori S, Nishimura N, Tani H, Mito T, et al. (2019). Acquired Expression of Mutant Mitofusin 2 Causes Progressive Neurodegeneration and Abnormal Behavior. *J Neurosci*. 39, 1588-1604. doi: 10.1523/JNEUROSCI.2139-18.2018.

Janakiraman U, Dhanalakshmi C, Yu J, Moutal A, Boinon L, Fukunaga K, et al. (2020). The investigation of the T-type calcium channel enhancer SAK3 in an animal model of TAF1 intellectual disability syndrome. *Neurobiol Dis.* 143, 105006. doi: 10.1016/j.nbd.2020.105006.

Kageyama Y, Hoshijima M, Seo K, Bedja D, Sysa-Shah P, Andrabi SA, et al. (2014). Parkin-independent mitophagy requires Drp1 and maintains the integrity of mammalian heart and brain. *EMBO J*. 33, 2798-2813. doi: 10.15252/embj.201488658.

Kostadinov D, Beau M, Blanco-Pozo M, Häusser M. (2019). Predictive and reactive reward signals conveyed by climbing fiber inputs to cerebellar Purkinje cells. *Nat Neurosci.* 22, 950-962. doi: 10.1038/s41593-019-0381-8.

Lackner LL and Nunnari J. (2010). Small molecule inhibitors of mitochondrial division: tools that translate basic biological research into medicine. *Chem Biol*. 17, 578-583. doi: 10.1016/j.chembiol.2010.05.016.

Levite M, Zelig D, Friedman A, Ilouz N, Eilam R, Bromberg Z, et al. (2020). Dual-Targeted Autoimmune Sword in Fatal Epilepsy: Patient's glutamate receptor AMPA GluR3B peptide autoimmune antibodies bind, induce Reactive Oxygen Species (ROS) in, and kill both human neural cells and T cells. *J Autoimmun*. 112, 102462. doi: 10.1016/j.jaut.2020.102462.

Louis ED and Faust PL. (2020). Essential tremor pathology: neurodegeneration and reorganization of neuronal connections. *Nat Rev Neurol*. 16, 69-83. doi: 10.1038/s41582-019-0302-1.

Luo TT, Dai CQ, Wang JQ, Wang ZM, Yang Y, Zhang KL, et al. (2020). Drp1 is widely, yet heterogeneously, distributed in the mouse central nervous system. *Mol Brain* 13, 90. doi: 10.1186/s13041-020-00628-y.

Muzumdar MD, Tasic B, Miyamichi K, Li L, Luo L. (2007). A global double-fluorescent Cre reporter mouse. *Genesis* 45, 593-605. doi: 10.1002/dvg.20335.

Oettinghaus B, Licci M, Scorrano L, Frank S. (2012). Less than perfect divorces: dysregulated mitochondrial fission and neurodegeneration. *Acta Neuropathol*. 123, 189-203. doi: 10.1007/s00401-011-0930-z.

Owens K, et al. (2013). Mitochondrial dysfunction and NAD(+) metabolism alterations in the pathophysiology of acute brain injury. *Transl Stroke Res.* 4, 618-634. doi: 10.1007/s12975-013-0278-x.

Pan MK, Li YS, Wong SB, Ni CL, Wang YM, Liu WC, et al. (2020). Cerebellar oscillations driven by synaptic pruning deficits of cerebellar climbing fibers contribute to tremor pathophysiology. *Sci Transl Med*. 12, eaay1769. doi: 10.1126/scitranslmed.aay1769.

Patron M, Sprenger HG, Langer T. (2018). m-AAA proteases, mitochondrial calcium homeostasis and neurodegeneration. *Cell Res*. 28, 296-306. doi: 10.1038/cr.2018.17.

Paxinos G and Franklin KBJ. (2001). *The Mouse Brain in Stereotaxic Coordinates*, 2ed edition, San Diego: Academic Press.

Peng TI and Jou MJ. (2010). Oxidative stress caused by mitochondrial calcium overload. *Ann N Y Acad Sci*. 1201, 183-188. doi: 10.1111/j.1749-6632.2010.05634.x.

Rizzuto R, De Stefani D, Raffaello A, Mammucari C. (2012). Mitochondria as sensors and regulators of calcium signalling. *Nat Rev Mol Cell Biol*. 13, 566-578. doi: 10.1038/nrm3412.

Singh-Bains MK, Linke V, Austria MDR, Tan AYS, Scotter EL, Mehrabi NF, et al. (2019). Altered microglia and neurovasculature in the Alzheimer's disease cerebellum. *Neurobiol Dis*. 132, 104589. doi: 10.1016/j.nbd.2019.104589.

Taniguchi H, He M, Wu P, Kim S, Paik R, Sugino K, et al. (2011). A resource of Cre driver lines for genetic targeting of GABAergic neurons in cerebral cortex. *Neuron* 71, 995-1013. doi: 10.1016/j.neuron.2011.07.026.

Wakabayashi J, Zhang Z, Wakabayashi N, Tamura Y, Fukaya M, Kensler TW, et al. (2009). The dynamin-related GTPase Drp1 is required for embryonic and brain development in mice. *J Cell Biol*. 186, 805-816. doi: 10.1083/jcb.200903065.

Wang F, Flanagan J, Su N, Wang LC, Bui S, Nielson A, et al. (2012). RNAscope: a novel in situ RNA analysis platform for formalin-fixed, paraffin-embedded tissues. *J Mol Diagn.* 14, 22-29. doi: 10.1016/j.jmoldx.2011.08.002.

Yawno T, Sutherland AE, Pham Y, Castillo-Melendez M, Jenkin G, Miller SL. (2019). Fetal Growth Restriction Alters Cerebellar Development in Fetal and Neonatal Sheep. *Front Physiol*. 10, 560. doi: 10.3389/fphys.2019.00560.

Zhang L, Wang H, Zhou X, Mao L, Ding K, Hu Z. (2019). Role of mitochondrial calcium uniporter-mediated Ca2+ and iron accumulation in traumatic brain injury. *J Cell Mol Med*. 23, 2995-3009. doi: 10.1111/jcmm.14206. Epub 2019 Feb 12.

Züchner S, Mersiyanova IV, Muglia M, Bissar-Tadmouri N, Rochelle J, Dadali EL, et al. (2004). Mutations in the mitochondrial GTPase mitofusin 2 cause Charcot-Marie-Tooth neuropathy type 2A. *Nat Genet*. 36, 449-451. doi: 10.1038/ng1341.

Tables

Table 1. The primers sequences and program were used to identify specific genotype.

	Primers for mutant type	Primers for wild-type allele
Gad2-cre	CTTCTTCCGCATGGTCATCT CACCCCACTGGTTTTGATTT	CTTCTTCCGCATGGTCATCT AAAGCAATAGCATCACAAATTTCA
ZsGreen-tdTomato$^{fl/fl}$	ATGCCCACCAAAGTCATCAGTGTAG AGGCGGGCCATTTACCGTAAGTTA	GGGCAGTCTGGTACTTCCAAGCT ATATCCCCTTGTTCCCTTTCTGC
Gad2^{tdTomato}/non-Gad2^{ZsGreen}	CTTCTTCCGCATGGTCATCT CACCCCACTGGTTTTGATTT ATGCCCACCAAAGTCATCAGTGTAG AGGCGGGCCATTTACCGTAAGTTA	CTTCTTCCGCATGGTCATCT AAAGCAATAGCATCACAAATTTCA GGGCAGTCTGGTACTTCCAAGCT ATATCCCCTTGTTCCCTTTCTGC

The PCR program used was as follows:

94°C for 3 min, then 35 cycles of 94°C for 30 s for denaturation, 62°C for 35 s for annealing, and 72°C 45 s for elongation.

Table 2. The antibodies were used to verify the purkinje cells in Gad2^{tdTomato}/non-Gad2^{ZsGreen} mice.

Antibody type	Antibody name	Mark for different cerebellar cells	Company	Product number	Dilution condition	Species
Primary antibody	**Anti-Calbindin**	**Purkinje cells**	Abcam	Ab75524	1: 500	Mouse
	Anti-NeuN	**Granule cells**	Abcam	ab177487	1: 500	Rabbit
	Anti-GFAP	**Astrocytes**	Cell Signaling	12389	1: 500	Rabbit
	Anti-Iba1	**Microglia**	Reagent	SKM6526	1: 500	Rabbit
Secondary antibody	**Dylight 649, Goat Anti-Rabbit IgG**	□	Abbkine	A23620	1: 500	Rabbit
	Dylight 649, Goat Anti-Mouse IgG	□	Abbkine	A23610	1: 500	Mouse
Nucleus dye	**DAPI**	□	Beyotime	C1005	1: 1000	□

Table 3. The probes were used in RNAscope in situ hybridization.

Name	Mitochondrial localization	Function	Accession number	Target region	Dilution	TSA® Plus channel
Drp1	OMM	Mitochondrial fission	NM_152816.3	793-1845	1 : 1	1
Mfn1	OMM	Mitochondrial fusion	NM_024200.4	1059-2413	1 : 1	1
Mfn2	OMM	Mitochondrial fusion	NM_001285920.1	795-1230	1 : 50	3
Mcu	IMM	Mitochondrial calcium intruder	NM_001033259.4	148-1206	1 : 50	2
Nclx	IMM	Mitochondrial calcium extruder	NM_133221.2	429-1459	1 : 50	3
Ucp2	IMM	Mitochondrial uncoupling	NM_011671.5	2-1002	1 : 1	1
Ucp4	IMM	Mitochondrial uncoupling	NM_028711.4	457-1410	1 : 50	3
Pcp2		Purkinje cell marker	NM_001129804.1	2-302	1 : 50	2
Polr2a	Positive control		NM_009089.2	2802-3678	1 : 1	1
PPIB	Positive control		NM_011169.2	98-856	1 : 1	2
UBC	Positive control		NM_019639.4	34-860	1 : 1	3
DapB	Negative control		EF191515	414-862	1 : 1	1, 2, 3

Drp1, dynamin-related protein; **MCU,** mitochondrial calcium uniporter; **Mfn1/2,** mitofusion 1/2; **NCLX,** sodium/lithium/calcium exchanger; **Pcp2,** Purkinje cell protein 2; **UCP2/4**, uncoupling protein 2/4. **IMM** = Inner mitochondrial membrane; **OMM** = Outer mitochondrial membrane

Table 4. Semi-quantitative assessment to visualize the target mRNA expression level both the dendrite shafts and soma with of Purkinje cells by binning the percentage of constructs

with a certain number of dots in one bin in cerebellum of Gad2-cre; ZsGreen-tdTomato$^{fl/fl}$ mice.

The number of bins ranges from 0 - 4 according to the ACD scoring system. The overall H score can range from 0 - 400 and was calculated as methods described in the Methods.

Figures

Mfn2 mRNA

	% of Dendrite Shafts	Dendritic Weighted Formula	% of Soma	Soma Weighted Formula
Bin 0 (0 Dots / dendrite or soma)	12	0 * 4	0	0 * 0
Bin 1 (1-3 Dots / dendrite or soma)	52	+ 1 * 52	1	+ 1 * 1
Bin 2 (4-9 Dots / dendrite or soma)	4	+ 2 * 4	1	+ 2 * 1
Bin 3 (10-15 Dots / dendrite or soma)	0	+ 3 * 0	8	+ 3 * 8
Bin 4 (>15 Dots / dendrite or soma)	0	+ 4 * 0	28	+ 4 * 28
H-Score		**60**		**139**

Mcu mRNA

	% of Dendrite Shafts	Dendritic Weighted Formula	% of Soma	Soma Weighted Formula
Bin 0 (0 Dots / dendrite or soma)	40	0 * 40	11	0 * 11
Bin 1 (1-3 Dots / dendrite or soma)	30	+ 1 * 30	18	+ 1 * 18
Bin 2 (4-9 Dots / dendrite or soma)	0	+ 2 * 0	2	+ 2 * 2
Bin 3 (10-15 Dots / dendrite or soma)	0	+ 3 * 0	0	+ 3 * 0
Bin 4 (>15 Dots / dendrite or soma)	0	+ 4 * 0	0	+ 4 * 0
H-Score		**70**		**22**

Nclx mRNA

	% of Dendrite Shafts	Dendritic Weighted Formula	% of Soma	Soma Weighted Formula
Bin 0 (0 Dots / dendrite or soma)	55	0 * 55	10	0 * 10
Bin 1 (1-3 Dots / dendrite or soma)	4	+ 1 * 4	21	+ 1 * 21
Bin 2 (4-9 Dots / dendrite or soma)	1	+ 2 * 1	5	+ 2 * 5
Bin 3 (10-15 Dots / dendrite or soma)	0	+ 3 * 0	0	+ 3 * 0
Bin 4 (>15 Dots / dendrite or soma)	0	+ 4 * 0	0	+ 4 * 0
H-Score		**4**		**31**

Ucp2 mRNA

	% of	Dendritic Weighted Formula	% of Soma	Soma

	Dendrite Shafts			Weighted Formula
Bin 0 (0 Dots / dendrite or soma)	3	0 * 45	0	0 * 15
Bin 1 (1-3 Dots / dendrite or soma)	13	+ 1 * 15	0	+ 1 * 15
Bin 2 (4-9 Dots / dendrite or soma)	1	+ 2 * 0	0	+ 2 * 6
Bin 3 (10-15 Dots / dendrite or soma)	0	+ 3 * 0	14	+ 3 * 0
Bin 4 (>15 Dots / dendrite or soma)	0	+ 4 * 0	3	+ 4 * 0
H-Score		**15**		**27**

***Ucp4* mRNA**

	% of Dendrite Shafts	Dendritic Weighted Formula	% of Soma	Soma Weighted Formula
Bin 0 (0 Dots / dendrite or soma)	3	0 * 3	0	0 * 0
Bin 1 (1-3 Dots / dendrite or soma)	14	+ 1 * 14	0	+ 1 * 4
Bin 2 (4-9 Dots / dendrite or soma)	0	+ 2 * 0	0	+ 2 * 4
Bin 3 (10-15 Dots / dendrite or soma)	0	+ 3 * 0	14	+ 3 * 25
Bin 4 (>15 Dots / dendrite or soma)	0	+ 4 * 0	3	+ 4 * 4
H-Score		**14**		**103**

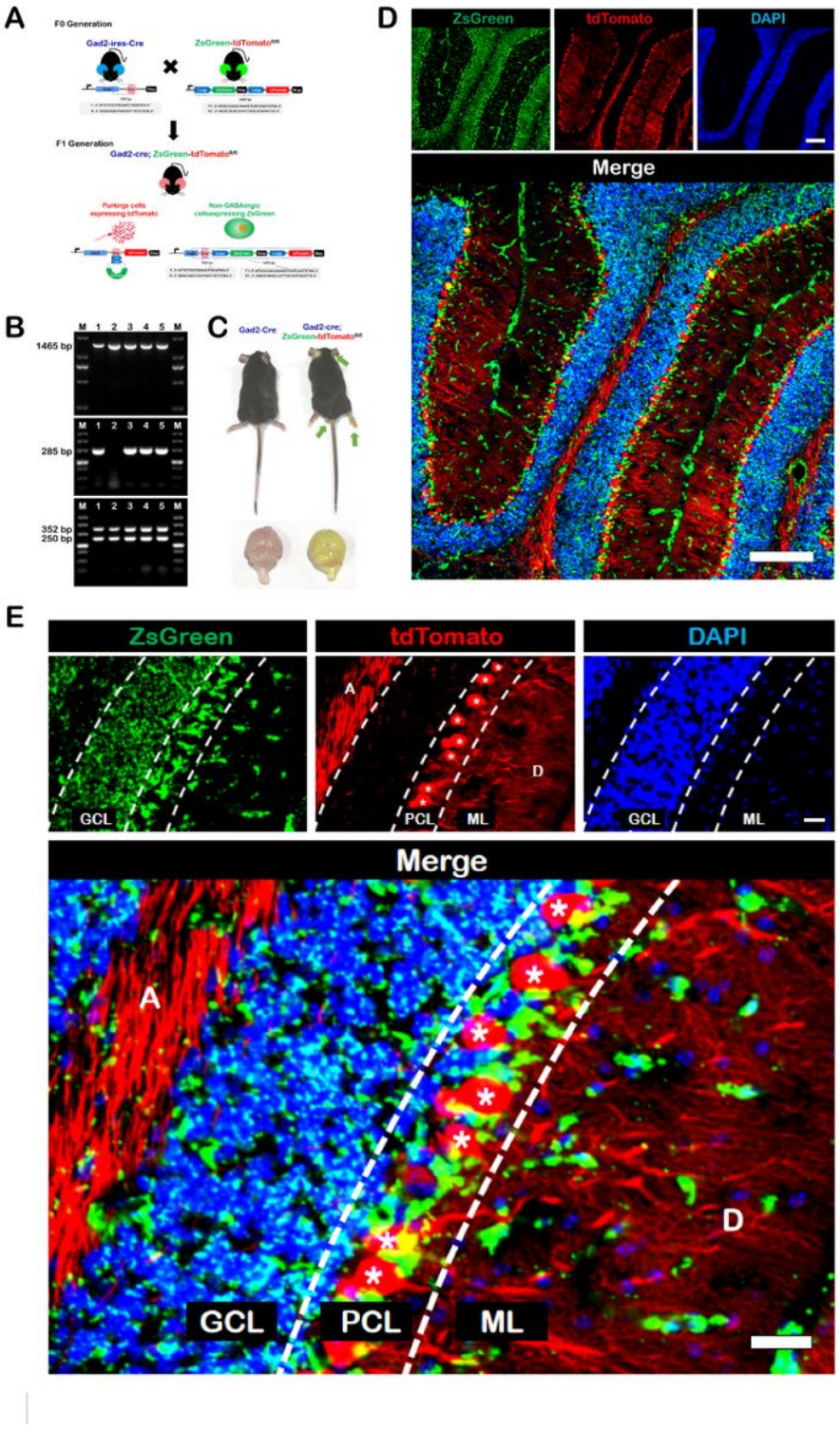

Figure 1

Purkinje cells specifically expressed tdTomato in GAD2-cre;ZsGreen-tdTomatofl/fl mice. (A) Strategy to generate a conditional knock-in mice with specific fluorescence in GABAergic Purkinje cell by using cre-loxP system. The Gad2-ires-Cre mice inserted an ires and a Cre recombinase sequence at the 3' end of the Gad2 allele, so that all of GABAergic neurons contained Cre recombinase. In the ZsGreen-tdTomatofl/f mice, ZsGreen and tdTomato were knocked in and the loxP sites were buried on both sides of ZsGreen.

After crossing of these two mice, all GABAergic neurons in the newly generated transgenic Gad2-cre;ZsGreen-tdTomatofl/fl mice would transfer from expressing ZsGreen to expressing tdTomato due to Cre recombinase cutting loxP sites. (B) Genotyping PCR results. The genotyping strategy used four sets of primers to produce four bands of 1465 bp (for ZsGreen-tdTomato with loxP site), 285 bp (for wild type site), 352 bp (Cre recombinase), and 250 bp (for for wild type site). So the mice numbered 1 and 3-5 in the picture with the four bands simultaneously, were Gad2-cre;ZsGreen-tdTomatofl/fl mice, who were used for the subsequent morphological observation. (C) The pictures of bodies (up) and brains (down) of control Gad2-cre and Gad2-cre;ZsGreen-tdTomatofl/fl mice at P21. Average body weights were 10.2 ± 0.8 g (Gad2-cre; n = 10) and 10.2 ± 1.0 g (Gad2-cre;ZsGreen-tdTomatofl/fl; n = 10), p = 0.80 (unpaired t test). Interestingly and apparently, Gad2-cre;ZsGreen-tdTomatofl/fl mice showed dazzling green light visible to the naked eye in external auricle skin (arrow), plantar skin (arrow), as well as perianal skin (arrow). It should be indicated that especially the brains of Gad2-cre;ZsGreen-tdTomatofl/fl mice showed green fluorescence, while the brains of control Gad2-cre mice showed normal pink, which made it very easy to distinguish the GABAergic knock-in mice. (D) Confocal microscope image of cerebellar Purkinje cells expressing tdTomato in the cerebellum of Gad2-cre;ZsGreen-tdTomatofl/fl mice, together with non-GABAergic cells (expressing ZsGreen) and DAPI (blue) . (E) The higher magnification of Figure D. It could be noted that the neuronal bodies of Prukinje cells with red fluorescence (asterisk marked in E) were aligned like dominos stacked throughout the PCL (Purkinje cell layer) like soldiers, also they had large dendritic arbors (D) like within the ML (molecular layer) and sent axons (A) like bright flame out off cerebellar cortex, therefore they left the dark area of GCL (granular cell layer) which were occupied by green non-GABAergic cells. A, axons; D, dendritic arbors; GCL, granular cell layer; ML, molecular layer; PCL, Purkinje cell layer. Scale bars: 200 μm (D and E).

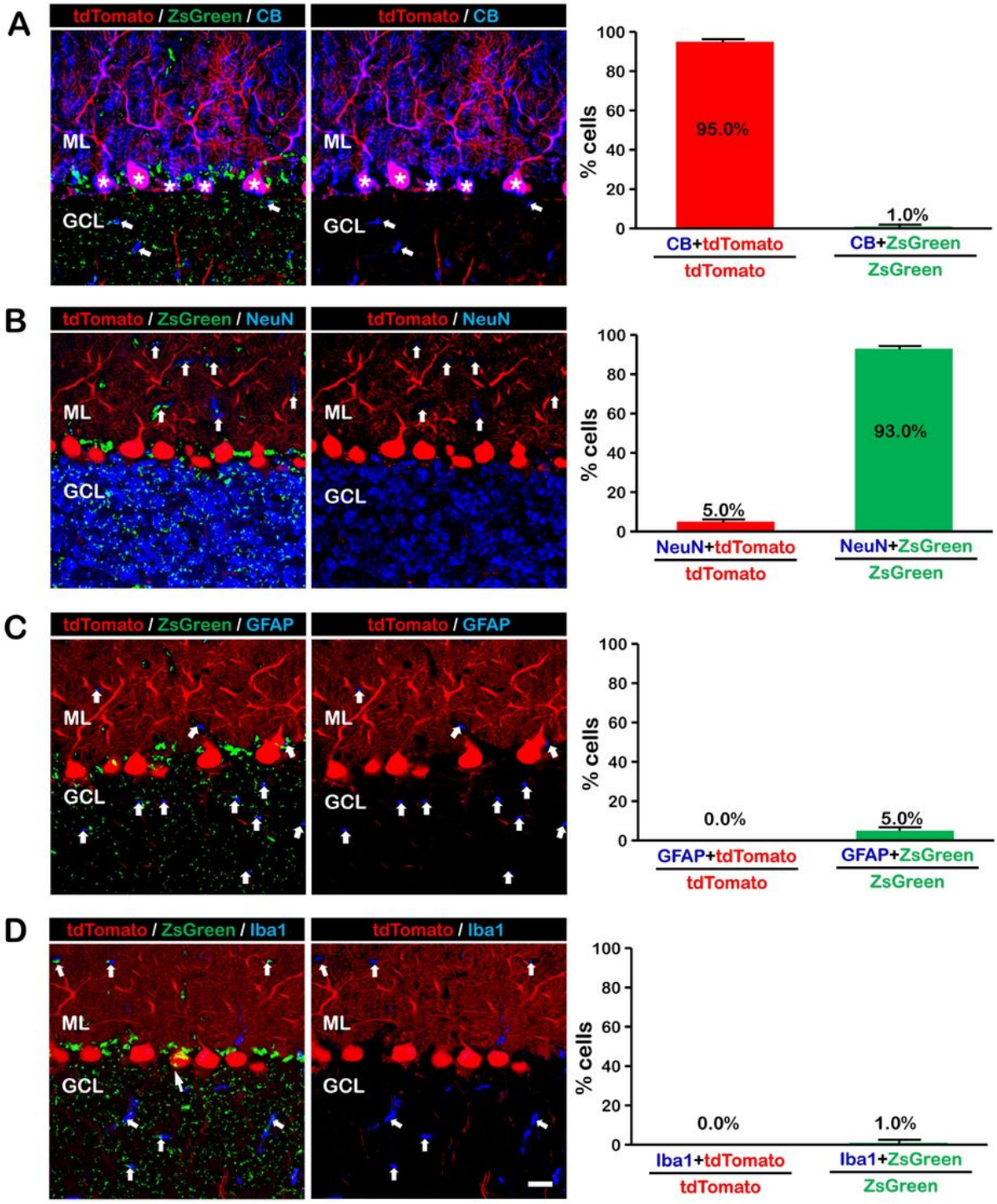

Figure 2

Double stainings verified Purkinje cells specifically expressing tdTomato fluorescence in GAD2-cre;ZsGreen-tdTomatofl/fl mice. (A) Left: tdTomato-positive cells (red) were almost 100% colocalized with calbinin (CB), the marker of Purkinje cells (marked by asterisk); Right: Percentage of cells with co-expressing in CB with tdTomato- or ZsGreen-positive cells in tdTomato- or ZsGreen-positive cells. Some arrows indicated that few CB-positive structures also scattered within GCL which consisted 1.0%

cololization of CB and ZsGreen. (B) Left: little tdTomato-positive cells (red) were colocalized with NeuN, the marker of granular cells; Right: Percentage of cells with co-expressing in NeuN with tdTomato- or ZsGreen-positive cells in tdTomato- or ZsGreen-positive cells. The arrows indicated that some NeuN-positive structures appeared in ML, but they did not colocalize with tdTomato fluorescence. (C) Left: none of tdTomato-positive cells (red) were colocalized with GFAP, the marker of astrocytes; Right: Percentage of cells with co-expressing in GFAP with tdTomato- or ZsGreen-positive cells in tdTomato- or ZsGreen-positive cells. The arrows indicated that some astrocytes appeared in both ML and GCL, but they did not colocalized with tdTomato fluorescence. (D) Left: none of tdTomato-positive cells (red) were colocalized with Iba1, the marker of microglia; Right: Percentage of cells with co-expressing in Iba1 with tdTomato- or ZsGreen-positive cells in tdTomato- or ZsGreen-positive cells. The arrows indicated that some microglia appeared in both ML and GCL, but they did not colocalized with tdTomato fluorescence. CB, Calbinin; GCL, granular cell layer; GFAP, Glial fibrillary acidic protein; ML, molecular layer; NeuN, Neuron specific nuclear protein; Scale bars: 20 μm.

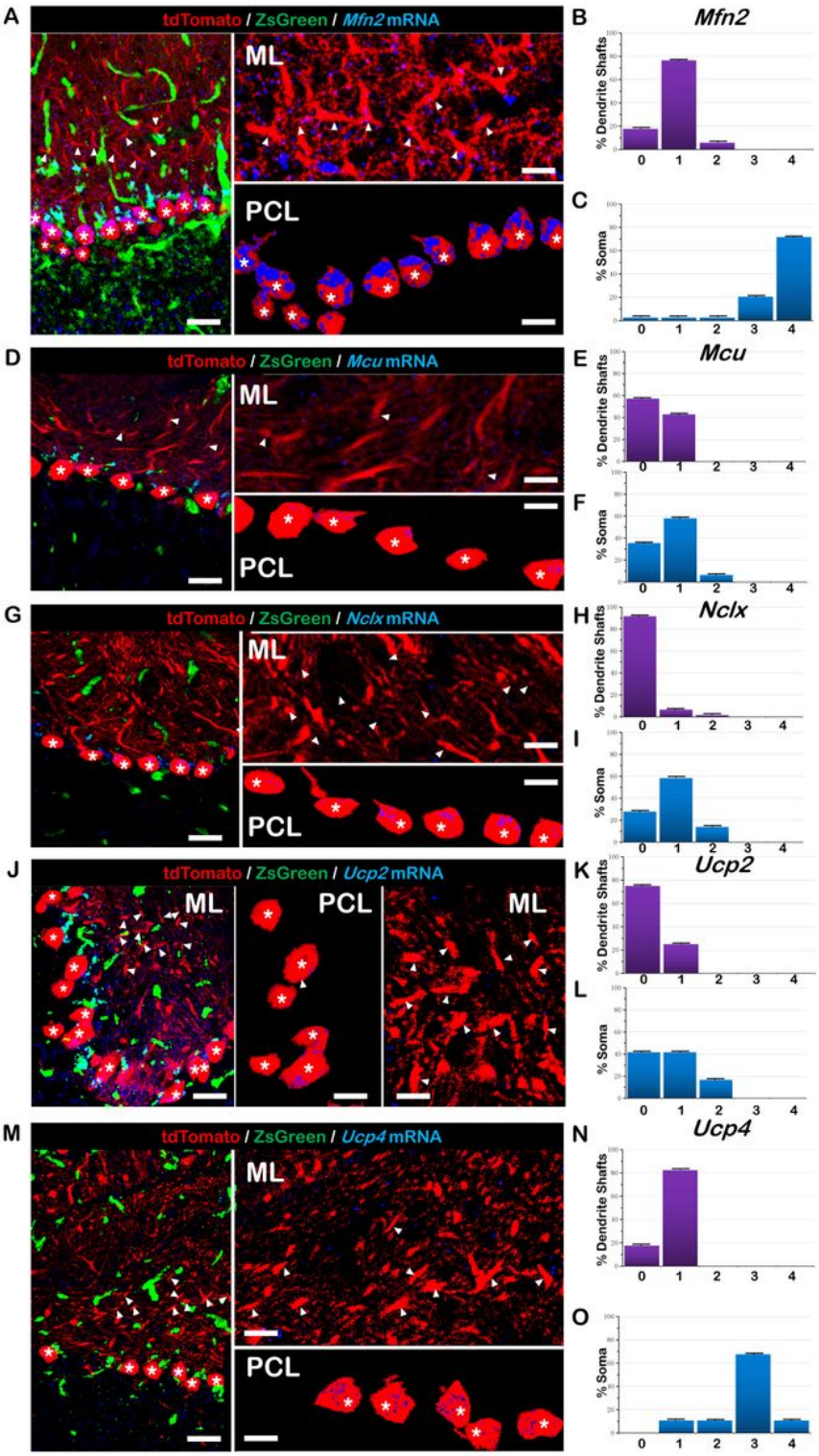

Figure 3

Identification of mRNAs of mitochondrial fusion, calcium transporter and uncoupling proteins (blue) in Purkinje cells (red) in the cerebellar cortex of GAD2-cre;ZsGreen-tdTomatofl/fl mice with RNAscope probes for Mfn2, Mcu, Nclx, Ucp2 and Ucp4 using the RNAscope. Green cells were non-GABAergic cells. Representative RNAscope images showing the expression of five types mRNAs (blue) for Mfn2 (A), Mcu (D), Nclx (G), Ucp2 (J) and Ucp4 (M) in Purkinje cells (red) were in left picture, whose higher magnification

images were shown in the relative right panels. In the right pictures, the expressions of mRNAs in dendrites were above marked by triangles within molecular layer (ML), while the expressions of mRNAs in soma were below marked by asterisk within Purkinje cell layer (PCL). The graph above showed that ACD quantification of mRNAS for Mfn2 (B), Mcu (E), Nclx (H), Ucp2 (K) and Ucp4 (N) in dendrite shafts. The graph below showed that ACD quantification of mRNAS for Mfn2 (C), Mcu (F), Nclx (I), Ucp2 (L) and Ucp4 (O) in soma. ACD, Advanced Cell Diagnostics; GAD, Glutamic acid decarboxylase; Mcu, Mitochondrial calcium uniporter; Mfn2, Mitofusion 2; ML, Molecular layer; Nclx, Sodium/lithium/calcium exchanger; PCL, Purkinje cell layer; Ucp2, Uncoupling protein 2; Ucp4, Uncoupling protein 4. Scale bars: 20 μm of the left panel (in A, D, G, J and M) and 200 μm of the right panel pictures (in A, D, G, J and M).

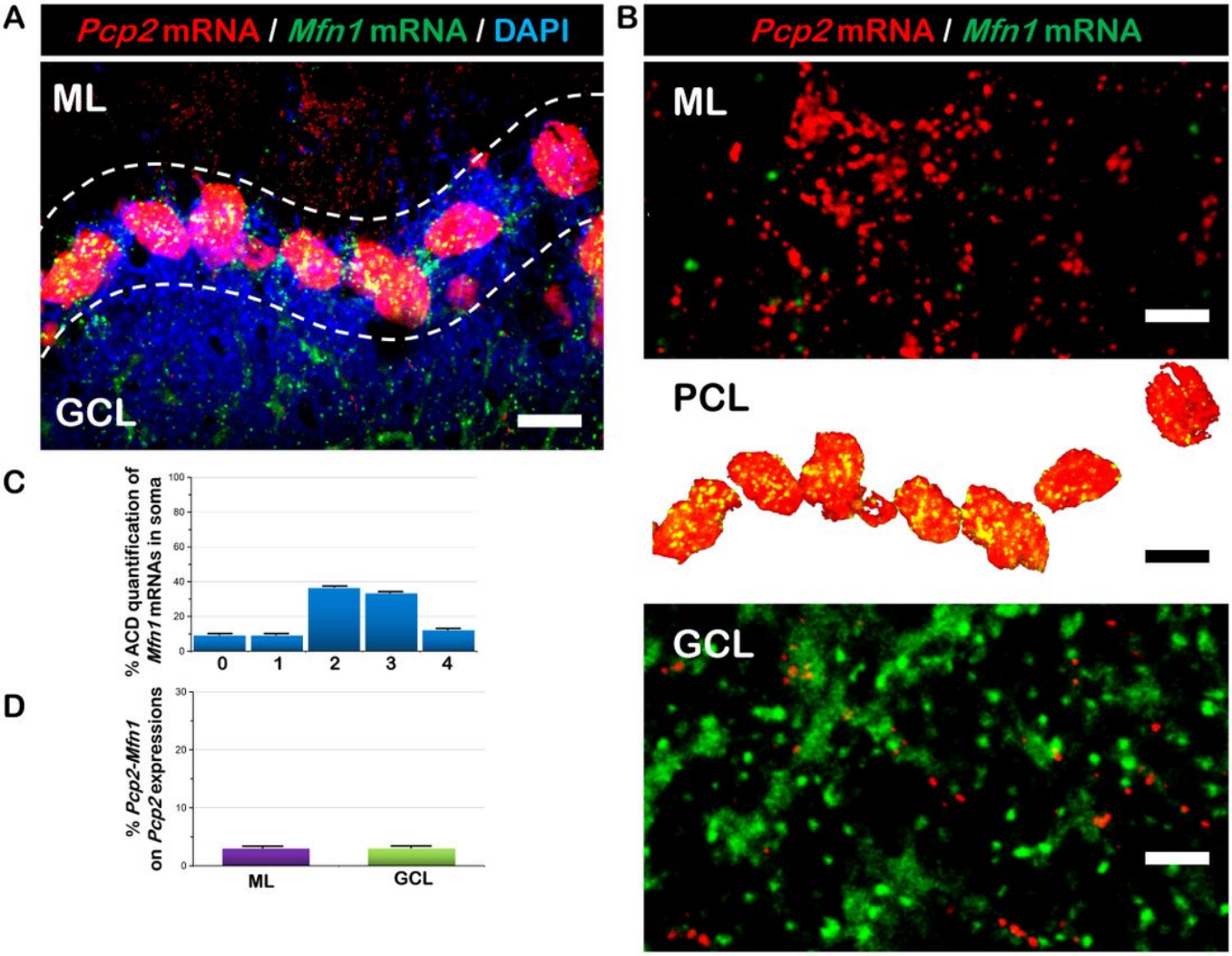

Figure 4

Detection of Mfn1 (green) and Pcp2 (red) in cerebellar cortex of C57BL/6 mice with the RNAscope Multiplex Fluoescent assay. (A) Representative RNAscope images showing the expression of Mfn1 mRNA (green) in Purkinje cells (red) which were distinguished by the red fluorescence with the mRNA probe of Purkinje cell protein-2 (pcp2) gene. Three layers of molecular layer (ML), Purkinje cell layer (PCL) and granular cell layer (GCL) are outlined with DAPI (blue). (B) Higher magnification images of Mfn1 (green)

and Pcp2 (red) RNAscopes in three layers of ML, PCL and GCL. Within the PCL, many yellow dots could be found in the soma of Purkinje cells (red). However, within both the ML and the GCL, few yellow dots could be found in the dendrites or axons of Purkinje cells, respectively. (C) The graph showed that ACD quantification of mRNAS for Mfn1 in soma. (D) The graph showed % double Pcp2-Mfn1 staining on Pcp2-positive expressions in ML and GCL. GCL, granular cell layer; pcp2, Purkinje cell protein 2; Mfn1, Mitofusion 1; ML, molecular layer; PCL, Purkinje cell layer. Scale bars: 20 μm (A and middle image of B); 200 μm (up and down images in B).

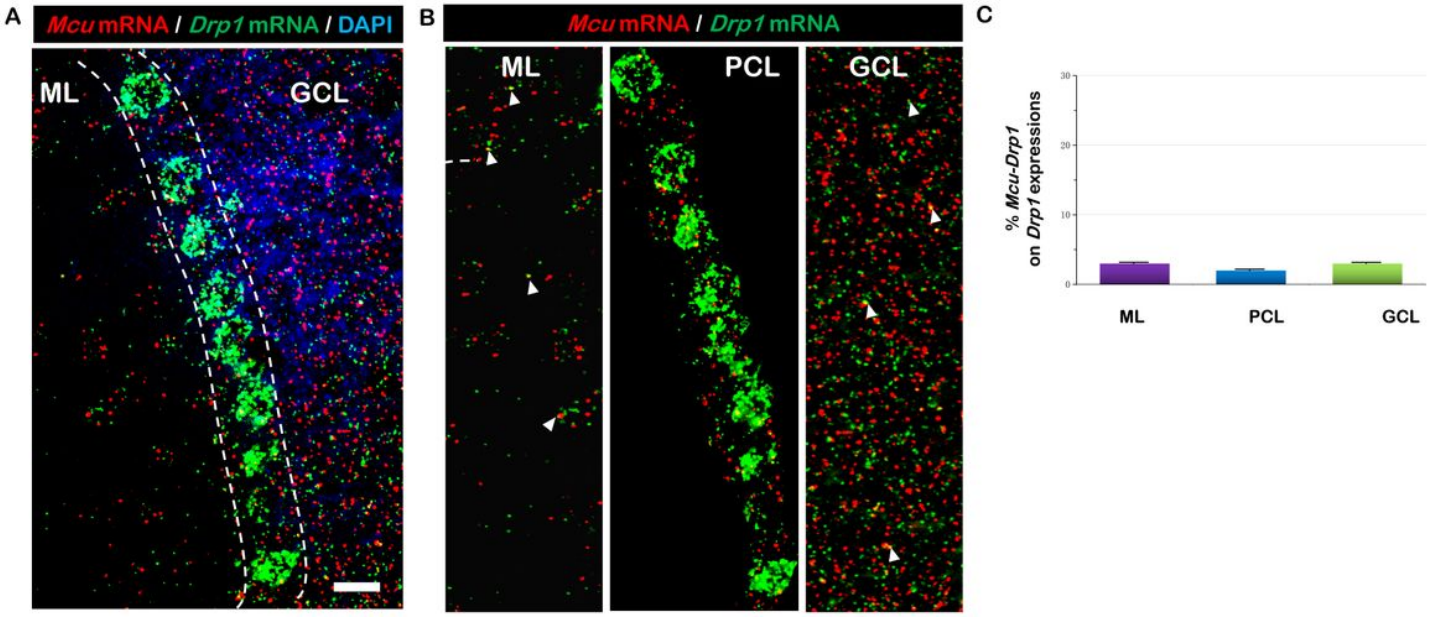

Figure 5

Detection of Drp1 (green) and Mcu (red) in cerebellar cortex of C57BL/6 mice with the RNAscope Multiplex Fluoescent assay. (A) Representative RNAscope images showing the expression of Mcu mRNA (red) in Purkinje cells (green) which were distinguished by the green fluorescence with the mRNA probe of Drp1 gene. Three layers of molecular layer (ML), Purkinje cell layer (PCL) and granular cell layer (GCL) are outlined with DAPI (blue). (B) Higher magnification images of Mcu (red) and Drp1 (green) RNAscopes in three layers of ML, PCL and GCL. Within the PCL, green dots of Drp1 could outline the soma of Purkinje cells. We found that very few red Mcu dots could be co-localizaed with green Drp1 dots (indicated by white triangles). (C) The graph showed % double Drp1-Mcu staining on Drp1-positive expressions in ML, PCL and GCL. Drp1, Dynamin-related protein 1; GCL, granular cell layer; Mcu, Mitochondrial calcium uniporter; ML, molecular layer; PCL, Purkinje cell layer. Scale bars: 20 μm (A and B).

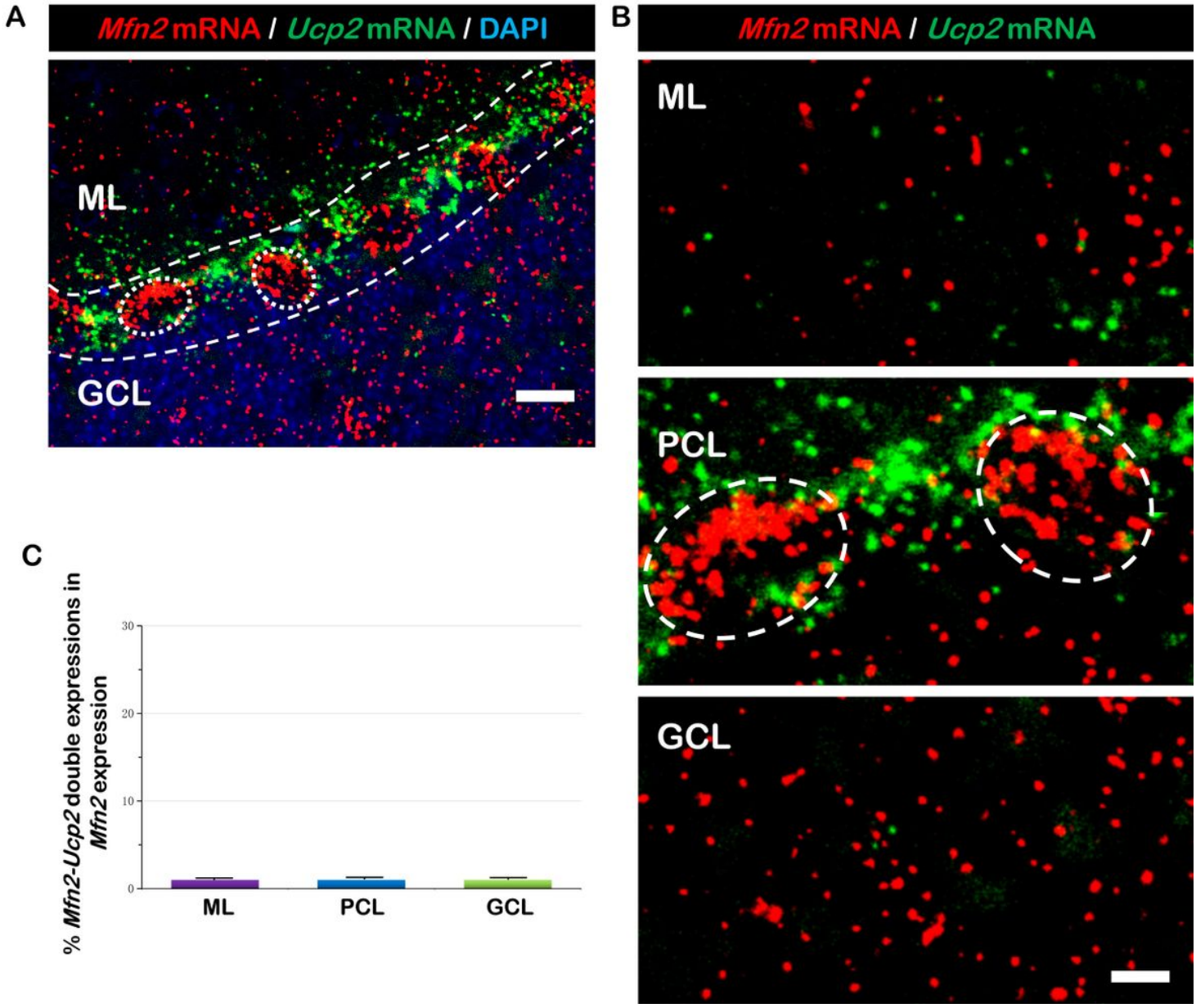

Figure 6

Detection of Ucp2 (green) and Mfn2 (red) in cerebellar cortex of C57BL/6 mice with the RNAscope Multiplex Fluoescent assay. (A) Representative RNAscope images showing the expression of Ucp2 mRNA (green) in Purkinje cells (red) which were distinguished by the red fluorescence with the mRNA probe of Mfn2 gene (circlered by white dotted line). Three layers of molecular layer (ML), Purkinje cell layer (PCL) and granular cell layer (GCL) are outlined with DAPI (blue). (B) Higher magnification images of Ucp2 (green) and Mfn2 (red) RNAscopes in three layers of ML, PCL and GCL. Within the PCL, red dots of Mfn2 could outline the soma of Purkinje cells (white dotted circled). We found that very few red Ucp2 dots could be co-localizaed with red Mfn2 dots (indicated by white triangles). (C) The graph showed % double Mfn2-Ucp2 staining on Mfn2-positive expressions in ML, PCL and GCL. GCL, granular cell layer; Mfn2, Mitofusion 2; ML, molecular layer; PCL, Purkinje cell layer; Ucp2, Uncoupling protein 2. Scale bars: 20 μm (A) and 2 μm (B).

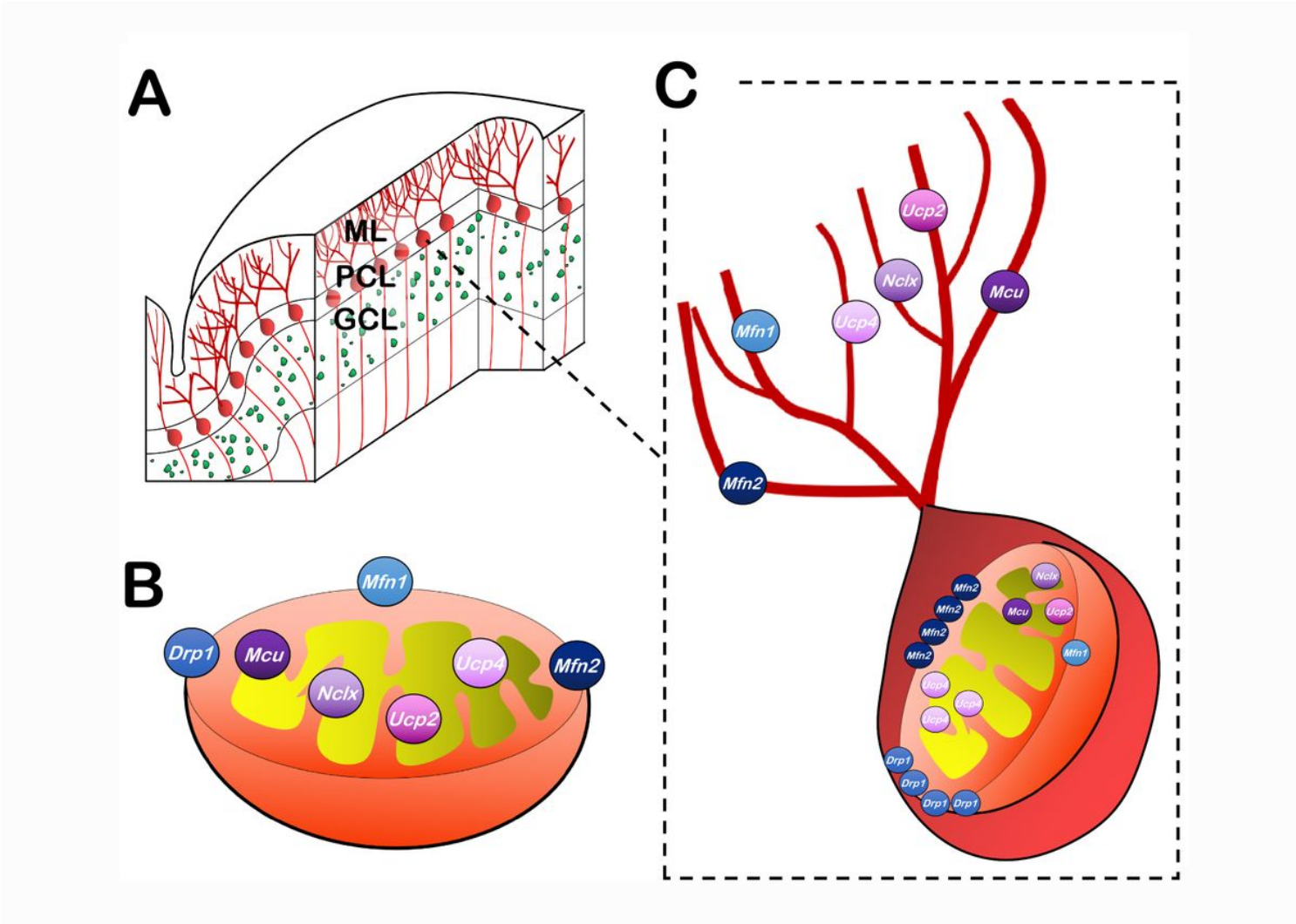

Figure 7

Proposed an convergence of 4 mitochondrial molecule mRNAs of DRP1/MFN2/MCU/UCP4 on soma of cerebellar purkinje cells by the present RNAscope in situ hybridization. (A) Our drawing of transverse section of a cerebellar folium, in which the dendrites, soma and axons of Purkinje cell painted as red were consist of three layers of molecular layer (ML), Purkinje cell layer (PCL) and granular cell layer (GCL), respectively. (B) Our drawing for pattern diagram of seven detected mitochondrial molecules including three on OMM of DRP1, MFN1 and MFN2 (colored blue) and four on IMM of MCU, NCLX, UCP2 and UCP4 (colored purple). (C) Our conclusion of an convergence of four mitochondrial molecule mRNAs for DRP1 and MFN2 on OMM, as well as MCU and UCP4 on IMM within soma of cerebellar Purkinje cells, although all of seven molecule could be present on Purkinje cells. DRP1, Dynamin-related protein 1; GCL, granular cell layer; IMM, Inner mitochondrial membrane; MCU, Mitochondrial calcium uniporter; MFN1, Mitofusion 1; MFN2, Mitofusion 2; ML, molecular layer; OMM, Outer mitochondrial membrane; PCL, Purkinje cell layer; UCP2, Uncoupling protein 2; UCP4, Uncoupling protein 4.

Supplementary Files

This is a list of supplementary files associated with this preprint. Click to download.

- sourcedataoffigure2.xlsx
- scoresoffigure3.xls
- scoresoffigure456.xls
- video1redandblue.wmv
- video2greenandblue.wmv
- video3greenredandblue.wmv